Temperature beneath continents as a function of continental cover and convective wavelength

Benjamin R. Philipps, Nicolas Coltice

JOURNAL OF GEOPHYSICAL RESEARCH, VOL. 115, B04408, doi:10.1029/2009JB006600, 2010

Temperature beneath continents as a function of continental cover and convective wavelength

Benjamin R. Phillips[1] and Nicolas Coltice[2]

Received 8 May 2009; revised 10 November 2009; accepted 24 November 2009; published 23 April 2010.

[1] Geodynamic modeling studies have demonstrated that mantle global warming can occur in response to continental aggregation, possibly leading to large-scale melting and associated continental breakup. Such feedback calls for a recipe describing how continents help to regulate the thermal evolution of the mantle. Here we use spherical mantle convection models with continents to quantify variations in subcontinental temperature as a function of continent size and distribution and convective wavelength. Through comparison to a simple analytical boundary layer model, we show that larger continents beget warming of the underlying mantle, with heating sometimes compounded by the formation of broader convection cells associated with the biggest continents. Our results hold well for purely internally heated and partially core heated models with Rayleigh numbers of 10^5 to 10^7 containing continents with sizes ranging from that of Antarctica to Pangea. Results from a time-dependent model with three mobile continents of various sizes suggests that the tendency for temperatures to rise with continent size persists on average over timescales of billions of years.

Citation: Phillips, B. R., and N. Coltice (2010), Temperature beneath continents as a function of continental cover and convective wavelength, *J. Geophys. Res.*, *115*, B04408, doi:10.1029/2009JB006600.

1. Introduction

[2] It is well accepted that Pangea is responsible for significant broadening of flow scales and warming in the mantle [*Anderson*, 1982; *Le Pichon and Huchon*, 1984]. Earlier supercontinents are also implicated in widespread warming events, evidenced by coincident large-scale magmatism [*Yale and Carpenter*, 1998; *Condie*, 2004]. If the largest continents have a clear insulative effect on the mantle, to what extent is this the same for smaller, distributed continents? Seismic models [e.g., *Woodhouse and Dziewoński*, 1984; *Dalton et al.*, 2008] and dynamic topography [*Hager and Richards*, 1989; *Ricard et al.*, 1993] do not suggest a dependence of subcontinental temperature on continent size today, with heterogeneity instead following largely from the distribution of subduction since the breakup of Pangea [e.g., *Ricard et al.*, 1993; *Anderson*, 1994; *Lithgow-Bertelloni and Richards*, 1998]. However, these snapshots tell us mostly of effects younger than 200 million years (Myr) and certainly depict only one state of a transient system. Characterizing the feedback between continent size and distribution, convective wavelength, and mantle temperature is therefore a worthwhile endeavor, the results of which could hold implications for the distribution of volcanism and the mantle cooling rate over Earth's history.

[3] A number of numerical and laboratory studies in a box or annulus have demonstrated the combined effects of continental coverage and broadening flow scale in raising mantle temperatures in models with a single continent or a pair of aggregating continents [e.g., *Gurnis*, 1988; *Zhong and Gurnis*, 1993; *Lowman and Jarvis*, 1993; *Lenardic and Kaula*, 1995; *Guillou and Jaupart*, 1995; *Trubitsyn and Rykov*, 1995; *Bobrov et al.*, 1999; *Lowman and Gable*, 1999; *Grigné and Labrosse*, 2001; *Lenardic et al.*, 2003; *Jellinek and Lenardic*, 2009]. Several investigators have examined similar effects and reached similar conclusions in spherical geometry [e.g., *Yoshida et al.*, 1999; *Phillips and Bunge*, 2005; *Zhong et al.*, 2007].

[4] More recently, *Grigné et al.* [2007a, 2007b] systematically measured heat flow as a function of Rayleigh number (Ra) and lid width in two-dimensional Cartesian models, concluding that continents should have a strong locally insulating effect. Increasing continent size and/or decreasing Ra was also found to force the flow from a so called free loop mode, in which convection away from the continent is driven by thermal buoyancy, to a fixed loop regime, where longer-wavelength flow is constrained by the model box size. For larger box aspect ratios it was found that even small continental caps can promote the development of large-scale convection, particularly as Ra increases.

[5] *Trubitsyn and Rykov* [2001] pioneered the inclusion of multiple moving continents in spherical shell models with

[1]Earth and Environmental Sciences Division, Los Alamos National Laboratory, Los Alamos, New Mexico, USA.
[2]Laboratoire de Sciences de la Terre, UMR 5570, Université Lyon 1, CNRS, Villeurbanne, France.

0148-0227/10/2009JB006600

an isoviscous mantle heated from below, demonstrating the viability of supercontinent cycles driven by continental forcing of convection. Recently, *Trubitsyn et al.* [2008] included internal heating and continent boundaries appropriate to the present-day Earth and reproduced behaviors typical of continental evolution. *Phillips and Bunge* [2007] also included internal heating and a viscously stratified mantle in spherical geometry and found that the ability of continents to exert strong control over the convective planform was enhanced for models with weaker plumes. Using similar models, *Coltice et al.* [2007, 2009] quantified the effect of continental aggregation on underlying temperature. They found that simply forming a supercontinent led to broad mantle warming on the order of 100°C in 100 Myr due to increased continental coverage and coincident long-wavelength flow.

[6] In this study we build on our earlier work on modeling multiple continents in spherical convection [*Phillips and Bunge*, 2007; *Coltice et al.*, 2007, 2009] through a systematic study of the effects of continent size, continent distribution, and convective length-scale changes on mantle temperature. We begin with a description of our numerical model in section 2. Section 3 then describes results for models with fixed continents. First, numerical results are presented and analyzed with attention to continental radius and convective wavelength. Then, we extend a simple analytic model to fit our parameter space and show that it nicely predicts trends in the numerical results. Section 4 shows results for a model with three mobile continents that confirms the time-averaged behavior suggested by the fixed continent models of section 3. Finally, in section 5 we discuss our results in the context of other modeling studies and the evolution of the real Earth.

2. Numerical Model

[7] We investigate the feedback between continental rafts and mantle convection using the spherical geometry code Terra [*Bunge and Baumgardner*, 1995; *Phillips et al.*, 2009]. Our models consist of solutions to the incompressible Navier-Stokes equations coupled with physically consistent continental rafts. The vigor of convection depends on the Rayleigh number, written for a mixed heating mode as

$$\mathrm{Ra} = \frac{\rho g \alpha (\rho H h^5 + q h^4)}{k \kappa \mu}, \tag{1}$$

where $\rho, H, q, k, \kappa, g, \alpha, \mu$ are the density, heat production per unit mass, basal heat flux, thermal conductivity, thermal diffusivity, gravitational acceleration, thermal expansivity, and viscosity, respectively, for a system of thickness $h = R_e - R_c$ (outer minus inner radius, or mantle depth in our numerical models). In our simulations, mantle viscosity is laterally homogeneous but radially stratified, with an increase of a factor of 30 between the upper and lower mantle applied gradually over a depth range of 100 km. Oceanic boundary layer regions have the same viscosity as the rest of the upper mantle. Apart from continents, mechanical boundary conditions for the mantle are free-slip and zero radial velocity on the outer and inner boundaries. A fixed temperature of T_e = 300 K is applied over the entire surface and in the case of purely internally heated models an insulating condition is used at the base. For models with mixed heating, the bottom boundary condition is changed from insulating to an isothermal value of T_c = 1900 K, yielding a balance of ~85% internal to ~15% basal heating based on relative heat fluxes at the surface and across the core mantle boundary.

[8] Continents are represented by d = 225 km thick [*Artemieva and Mooney*, 2001; *Gung et al.*, 2003] circular lids, and we consider models both with fixed continents and continents that are free to move in response to convective tractions. Zero vertical velocity is applied throughout each continent, amounting to perfect buoyancy. For mobile continents, we use a torque balance approach following *Gable et al.* [1991], modified for the sphere [*Monnereau and Quéré*, 2001] and to advect the location of each continent through the grid according to the velocity solution [*Phillips et al.*, 2009]. Continents are therefore also perfectly rigid, with either a zero velocity condition or a uniform Euler rotation throughout for fixed and mobile continent cases, respectively. Heat flow through our model continents is about 45% of that through the oceanic regions. This is reasonably close to what is observed for the Earth [*Sclater et al.*, 1980] and is a simple byproduct of the imposed, thick continental boundary layer. See *Phillips et al.* [2009] for a more detailed description of our formulation for continental motion. The radial arc length of continents $a/2$ is varied between 2000 and 7400 km (roughly present-day Antarctica to Pangea in area). Nondimensional continental thickness and radii are then

$$d' = d/h = 0.078 \tag{2}$$

and

$$a'/2 = a/2h = 0.7 \text{ to } 2.56, \tag{3}$$

respectively. The transit or convective timescale $t_c = (h^2/\kappa)\,\mathrm{Ra}^{-2/3}$ [*Davies*, 1999] is taken as characteristic, such that nondimensional times reported for the mobile continent model are given by

$$t' = t/t_c = \left(\kappa/h^2\right)\mathrm{Ra}^{2/3} t. \tag{4}$$

[9] We ran 65 calculations with variations in continent size and number, mantle heating mode, and Ra. The mobile continent model, with Ra = 10^7, was run until a statistical steady state was reached (heat input balanced on average by heat output) and then for an additional period of 300 nondimensional time units. Since Ra for the Earth is likely between 10^8 and 10^9 [*Turcotte and Schubert*, 2002], equation (4) tells us that this would scale to a few billion years (Gyr). The various continental configurations employed in fixed continent models are shown in Figure 1. In models with a single continent the raft is fixed at the north pole. Pairs of equally sized continents are fixed at opposite poles. Additional models employ three different sized continents placed at 90° on center from one another. Total continental cover never exceeds 30% of the surface. These models were run for a scaled time period on the order of 1 Gyr beyond the

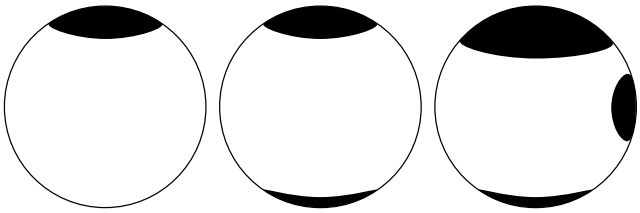

Figure 1. Example configurations for fixed continent models. Continents are shown as black discs on the surface of the spherical domain. A single continent is fixed at the north pole, pairs of equally sized continents are placed at opposite poles, and groups of three continents of differing size are placed at 90° on center to one another.

steady state. Values for fundamental model parameters are summarized in Table 1.

3. Fixed Continent Models

3.1. Continent Size

[10] Results for a subset of models with a purely internally heated mantle and Ra = 10^5 are shown in Figure 2. Plotted are average temperatures at a nondimensional depth of 0.18 in the upper mantle as a function of the total number of continents in the model and individual continent size. An open square is plotted for each continent in a given simulation. Error bars represent one standard deviation of temperature beneath each continent over the entire steady portion of each time-dependent convection calculation. We see that subcontinental temperature increases with continent size, but is independent of the total number of continents in a model.

[11] Figure 3 is the same as Figure 2, except that it is for models that are either purely internally heated (black squares) or 15% core heated (gray triangles) with Ra = 10^7. Subcontinental temperature still increases with continent size, mostly independent of the number of continents in the model. Temperatures beneath small, $a'/2 = 0.994$ (2880 km) continents sometimes lie above the expected trend. In these cases the small continent is in relatively close proximity to a larger continent in the same model (see Figure 1).

3.2. Convective Wavelength

[12] To complement our observations of subcontinental temperatures we monitored the fundamental scales of mantle flow. Figure 4 shows the time-averaged spectral heterogeneity of the mantle temperature field for a subset of the internally heated, Ra = 10^5 models. We plot depth-averaged root mean square spectral amplitude over spherical harmonic degrees 0–16 as a function of continent size. Each trace is normalized independently. Solid lines are for cases with a single continent while dashed lines correspond to cases with two continents. Significant power exists at shorter wavelengths above degree 4 for models containing the smallest continents. For continents of radius $a'/2 > 1.42$ the longest wavelengths at degrees 1 and 2 become dominant.

[13] In Figure 5 we plot the same spectral information for internally heated, Ra = 10^7 models. Here, smaller-scale structure is still evident in models with smaller continents, but spectral amplitude peaks at the longest wavelengths independent of continent size. Models with one continent exhibit a peak at degree 1, while two continent models peak at degree 2.

[14] A look at mantle temperature fields further illustrates some of the observations gleaned above. In Figure 6 we show snapshots for eight of our purely internally heated models, covering a parameter space including Ra = 10^5 and 10^7 and one or two continents sized at $a'/2 = 0.994$ or 1.75. Continents, located at the poles, are shown as translucent caps. The inner spherical boundary is the core-mantle boundary, the outer boundary shows mantle structure at the base of the continents, and a section is removed revealing a cross section through the mantle. Red features are hot and blue features are cold. In Figure 6a, we see that at low Ra, multiple convection cells persist independent of the single $a'/2 = 0.994$ continent. Figure 6b is similar, though with a second continent at the opposite pole. Moving to Figure 6c, a larger $a'/2 = 1.75$ continent has clearly imposed long-wavelength flow, verifying the inferred spectral shift seen in Figure 4. Adding a second large continent (Figure 6d) leads to an opposing upwelling and the development of degree two flow. Figure 6e shows the prevalence of smaller-scale features with the shift to higher Ra. It is not easy to pick out the underlying long-wavelength flow here or in Figure 6f because the small-scale structures are almost as strong (Figure 5). In Figure 6g, the long-wavelength flow forced by a larger continent grows in strength over the background fine-scale structure. As at lower Ra, the introduction of a second large continent brings with it a second large convection cell (Figure 6h).

3.3. Boundary Layer Model

[15] The temperature beneath a rigid cap is higher because of two effects: insulation and the enlargement of the convective wavelength. Insulation comes from forcing diffusion over a large depth range because of cap rigidity. Hence, most of the heat is removed away from the cap where the boundary layer is thinner. The presence of a rigid cap and/or layered viscosity forces larger-wavelength flow as well and,

Table 1. Model Parameters

Parameter	Value
R_e, outer shell radius	6370 km
R_c, inner shell radius	3480 km
T_e, surface temperature	300 K
T_c, basal temperature[a]	1900 K
H, internal heating rate	3.0×10^{-12} W kg^{-1}
ρ, reference density	4500 kg m^{-3}
g, gravity	9.8 m s^{-2}
k, thermal conductivity	2.4 W m^{-1}K^{-1}
κ, thermal diffusivity	5.3×10^{-7} m^{2}s^{-1}
α, thermal expansivity	2.5×10^{-5} K^{-1}
μ, viscosity[b]	1.1, 11, or 110 $\times 10^{22}$ Pa s
Ra, Rayleigh number[c]	10^5, 10^6, or 10^7
d, continental thickness	225 km
$a/2$, continental radii[d]	2000 to 7400 km
d', nondimensional thickness	0.078
$a'/2$, nondimensional radii	0.7 to 2.56

[a]Applicable for mixed internal/basal heating models. The inner boundary is insulating for models with internal heating only.

[b]Upper mantle viscosity. Viscosity increases by a factor of 30 from the upper to lower mantle.

[c]Volume-averaged value for pure internal heating.

[d]Continents are circular with sizes ranging from 2.5% to 30% of the surface, or roughly present-day Antarctica to Pangea.

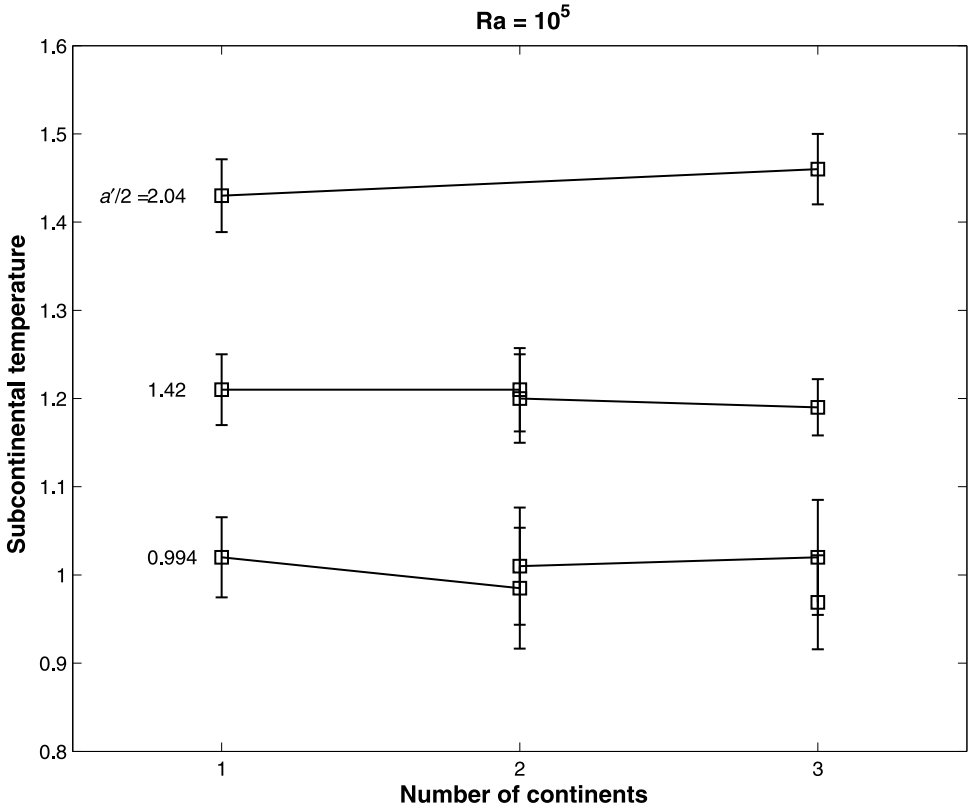

Figure 2. Nondimensional subcontinental temperature as a function of the number of continents in the model for various nondimensional continental radii $a'/2$ with pure internal heating and Ra = 10^5. Plotted are average temperatures over individual continental footprints below the thermal boundary layer at a nondimensional depth of 0.18 in the upper mantle. Error bars represent one standard deviation. Temperature is roughly constant for a given continent size, regardless of the number of continents.

as a consequence, the convective heat transfer is less efficient. To better distinguish between these two effects, we developed a simple boundary layer model for a cell heated both from within and from below and partially capped by a conducting lid (Figure 7).

[16] In this model, the horizontal and vertical velocity components vary linearly with the distance and depth, reaching maximum values u and v at the top and sides, respectively. Mass conservation requires

$$uh = v\frac{\lambda}{2}. \tag{5}$$

[17] We can compute the temperature distribution in the boundary layer assuming the velocity is constant throughout its depth. Following *Turcotte and Schubert* [2002], the rate of heat generation within a convection cell plus the basal heat flow equals the surface heat flow. Assuming heat flow through a continent of size a (diametric arc length in our spherical models) is negligible (this is the insulation effect), the balance of the heat sources (left-hand side) and the heat loss (right-hand side) is

$$\frac{\rho Hh\lambda + q\lambda}{2} = 2k\Delta T\left(\frac{u(\lambda - a)}{2\pi\kappa}\right)^{1/2}, \tag{6}$$

where ΔT and u are temperature change across the cell depth and surface velocity, respectively, for a system of length λ. Balancing viscous and buoyancy forces over the cell yields

$$\rho g\alpha\Delta Tu\left(\frac{\kappa\lambda}{2\pi u}\right)^{1/2} = \frac{4v^2\mu}{\lambda} + \frac{u^2\lambda\mu}{h^2}, \tag{7}$$

where v is the vertical convective velocity. Combining equations (5)–(7) yields

$$\Delta T = \left(\frac{\pi}{2}\right)^{1/2}\frac{\rho Hh^2 + qh}{k}\frac{\left(1 + (\lambda/2h)^4\right)^{1/4}}{((\lambda - a)/2h)^{1/2}}\mathrm{Ra}^{-1/4}. \tag{8}$$

[18] The nondimensional convective length scales and temperatures reported in our results are then given by

$$\lambda' = \lambda/h, \tag{9}$$

and

$$T' = \frac{k}{\rho Hh^2 + qh}\mathrm{Ra}^{1/4}T, \tag{10}$$

where the above follows from equation (8).

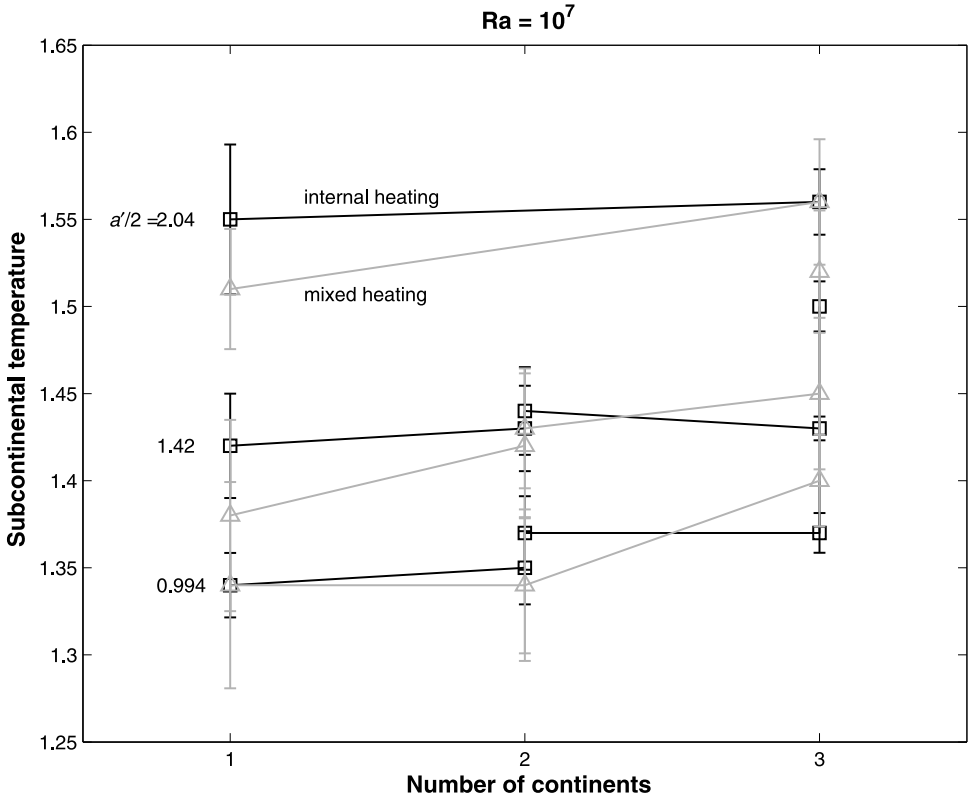

Figure 3. As in Figure 2, except for both purely internally heated (black squares) and 15% core heated (gray triangles) models with Ra = 10^7. Temperature is roughly constant for a given continent size, mostly independent of the number of continents. High temperatures for some $a'/2 = 0.994$, $N = 3$, mixed heating models signify additional heating of the mantle beneath the small continent due to the proximity of a larger continent.

[19] This model is built in Cartesian geometry. Expanding similar scalings to spherical geometry requires numerical solutions, and little work has yet been done to build spherical analytical boundary layer models [*van Keken*, 2001]. Our analytical model is simplified, both in terms of geometry and its treatment of convection. We therefore tune the trends predicted by this model for comparison with our numerical results. Solutions to equation (8), nondimensionalized using equation (10), are further multiplied by a constant factor, $A = 0.37$, that accounts for the geometry and complexity of the problem. Owing to the difference in upper and lower boundary areas in a spherical shell, geometry should become more of a factor as the proportion of heating from the core increases with respect to that from internal mantle sources. Since the mantle is heated predominantly from within and our numerical models include at most 15% core heating, the Cartesian approximation with the above scaling factor is a reasonable starting point for our study.

[20] We compared all of our model results with predictions of the boundary layer model. Figure 8 shows subcontinental temperatures as a function of continent size for the purely internally heated, Ra = 10^5 cases. Plotted over the data are the nondimensionalized, scaled (using A) solutions to equation (8) for cells of width $\lambda'/2 = 1.4$, 3.8, and 6.25 (corresponding to 4000, 11,000, and 18,000 km). Temperatures beneath the smallest continents fall near the trend for the narrowest boundary layer cell. This correlates with the blue spectrum observed for this case (Figure 4). As continent size increases, underlying temperature approaches the trend for midsized cells, commensurate with the reddening of the spectra for these models. As continental radius increases past $a'/2 = 1.42$, temperatures reach the trend for the broadest cell, again matching the spectral trends.

[21] Figure 9 demonstrates transitional behavior for models with internal or mixed heating at Ra = 10^6. With trends from equation (8) plotted for the same values of $\lambda'/2$ as in Figure 8, we see that none of the subcontinental temperature values correspond to the narrowest cell. For larger continents there is a clear transition to the trend for the largest cell.

[22] For Ra = 10^7, Figure 10 shows that subcontinental temperature falls along the trend for convection on the longest wavelength regardless of continent size. In fact, slightly higher temperatures for this case map to a wavelength of $\lambda'/2 = 7.6$ (22,000 km), a bit longer and therefore less efficient at removing heat than that found to fit the lower-Ra cases. This agrees with the result that large-scale flow dominates in our high-Ra models independent of continental radius (Figure 5). At high Ra it is then insulation that dominates since the key convective wavelength is almost constant. Outlying points at $a'/2 = 0.994$ correspond

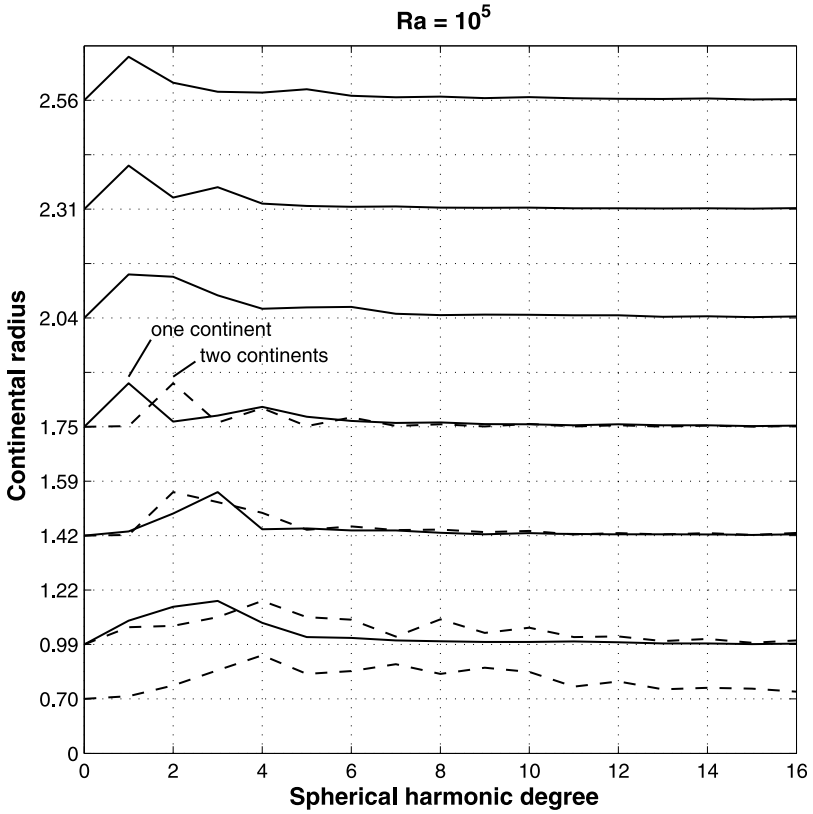

Figure 4. Time-averaged spectral heterogeneity of mantle temperature as a function of nondimensional continental radius for purely internally heated models with Ra = 10^5. Depth-averaged root mean square spectral amplitude is plotted for spherical harmonic degrees 0–16. Each trace is normalized independently. Solid and dashed lines represent cases with one or two continents, respectively. Power persists at shorter wavelengths (larger spherical harmonic degrees) for smaller continent sizes, suggesting that small-scale structure is strong until continent size reaches a critical value ($a'/2 > 1.42$).

to cases where small continents are affected by proximal, larger continents.

4. Mobile Continents

[23] All of the models discussed above have fixed continents. We saw in Figure 3 that continental distribution can affect underlying temperature. To study this effect we ran a model containing three mobile continents with $a'/2 = 1.75$, 1.42, and 0.994. The mantle is 15% core heated and the Rayleigh number is 10^7. Figure 11 shows nondimensional underlying temperature for each continent and the remaining, or oceanic regions, as a function of time. Triangles on the right mark the time-averaged temperature beneath each region. It is notable that these average values fall on the trend found in the fixed continent models and the boundary layer model (black circles, Figure 10). At the top, time periods during which continents were aggregated are bracketed by arrows and labeled with black discs representative of the area of the continents in contact. So, all three continents are joined at $t' = 0$, the small continent rifts away leaving the two larger continents joined at about $t' = 5$, and so on. There is significant time dependence in subcontinental temperature. However, on average temperature still increases with continent size. The half-period over which significant variations occur also increases with continent size, from as little as about 10 for the small continent to about 50 time units (roughly 500 Myr) for the large continent, which is comparable to the timescale over which continents aggregate or split up. We can also see that in some cases subcontinental temperature increases during periods of aggregation, as for the two smaller continents around $t' = 90$ and 250 and the small and large continents near $t' = 150$. The small continent also contacts the large continent at $t' = 280$, registering associated warming. Because the initial temperature beneath the small continent is lower than that beneath the larger one, its warming upon aggregation is also larger, although both continents approach the same final temperature. Finally, we note that the mantle just beneath continents is always warmer than the suboceanic mantle at the same depth, except in limited circumstances for the smallest continent (near $t' = 110$ and 220).

5. Discussion

5.1. Model Simplifications

[24] We have presented models that focus on the mechanical and thermal effects of simple conducting lids on convection in a spherical shell. These models incorporate a number of simplifying assumptions that reflect hurdles that the geodynamics community has yet to overcome in simu-

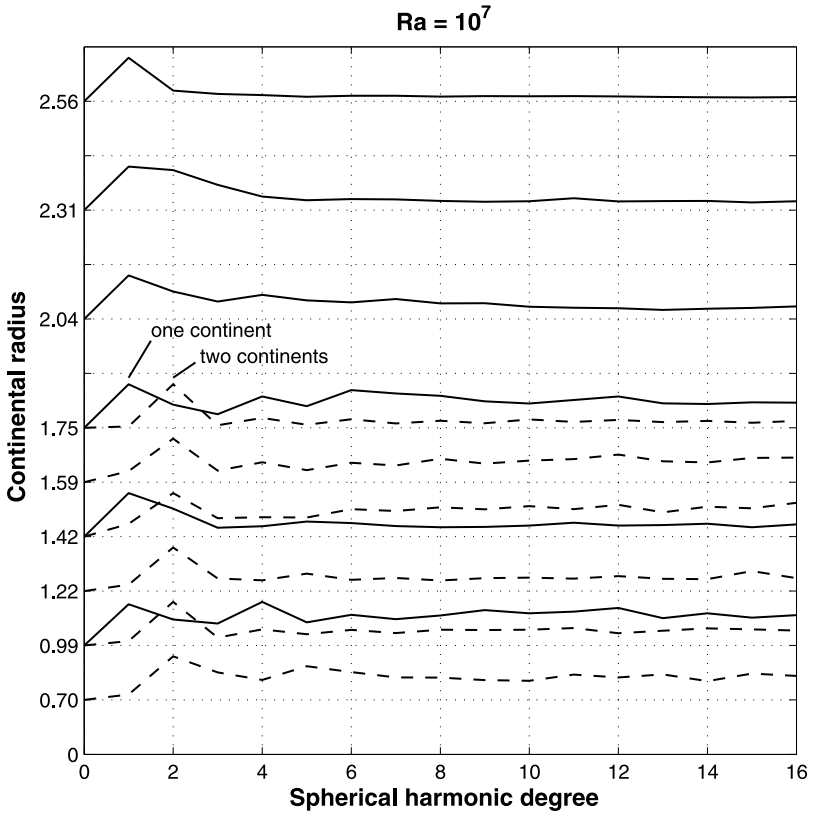

Figure 5. As in Figure 4, except for purely internally heated models with Ra = 10^7. Single continent cases exhibit a peak amplitude at degree 1, while two continent cases peak at degree 2, signifying the development of a broad convection cell associated with each continent independent of continent size.

lating some fundamental Earth-like processes on a global scale. Our models apply a free-slip boundary condition over the noncontinental surface regions. As a result, they lack the influence of large oceanic plates, which may also modify convective wavelength and hence mantle temperatures [e.g., *Bunge and Richards*, 1996; *Lowman and Gable*, 1999; *Monnereau and Quéré*, 2001]. However, studies such as *Bunge and Richards* [1996] and *Monnereau and Quéré* [2001] impose plate geometry and hence to a large degree predominant convective wavelengths. While three-dimensional models with formulations that approximate globe covering, evolving plate-like behavior are progressing [*Gait et al.*, 2008; *van Heck and Tackley*, 2008], no such model yet incorporates the effect of stable continents. Since our aim here is to focus on the influence of continents and evolving heterogeneity scales, we are relegated to using a free-slip condition in oceanic regions.

[25] Viscosity in our models is radially stratified, but does not vary with temperature. Temperature-dependent viscosities decrease in response to mantle heating, stimulating convection and eventually leading to cooling [*Lenardic et al.*, 2005; *Jellinek and Lenardic*, 2009]. Our numerical and analytical models do not include this self-regulating effect, possibly allowing for higher average temperatures. However, this effect presumes that subcontinental warming occurs in the first place, as these other authors do find. Temperature-dependent viscosity can also affect convective wavelength. In models that attempt to emulate the Earth in producing plate-like behavior, such complex rheologies yield convection at the longest wavelengths [e.g., *Tackley*, 2000]. Our combination of depth-dependent viscosity and continental plates also yields long-wavelength convection, so despite a simplified rheology our models do capture the appropriate range of length scales. It will be of great value to extend studies like the one presented here by incorporating more realistic rheological formulations. We hope that by capturing first-order characteristics, our models will serve to inform the interpretation of more complex systems as their simulation becomes tractable.

[26] Another modulating effect for temperature in the real Earth is the enrichment of continental material, and conversely the depletion of the mantle, in heat producing elements. The rate of heat production in our model mantle is constant despite the varying continental cover. While continental growth could help to cool the mantle by preferentially removing radiogenic products, increasing continent size leads to increased mantle temperatures even with the inclusion of this effect [*Cooper et al.*, 2006]. And, despite the fact that our continents are not enriched, they effectively cut conductive heat flow in half as compared to uncapped regions by virtue of their simple mechanical formulation, mirroring the ratio held between modern continental and oceanic lithosphere [*Sclater et al.*, 1980].

[27] The thermal budget of the Earth is poorly constrained. While we know that the mantle is heated primarily from within due to the decay of radioactive elements

[*Wasserburg et al.*, 1964], estimates for the proportion of heat entering the mantle from the core range from as little as 5% [e.g., *Davies*, 1988] to as high as perhaps 30% [e.g., *Kellogg et al.*, 1999; *Buffett*, 2002; *Bunge*, 2005; *Nolet et al.*, 2006]. We chose here a middle ground of 15% bottom heating to 85% internal heating. Due to the already exhaustive computational demands of the 65 calculations performed for this study, we focused on exploring continental distribution at this single mixed-heating mode. Shifting the balance toward more bottom heating would yield stronger plumes that can alter continental motions [*Phillips and Bunge*, 2007]. However, we do not expect that this would affect the fact that heat accumulates beneath continents, or the nondimensionalized warming trends that fit both the purely internally heated and 15% bottom heated models of this study.

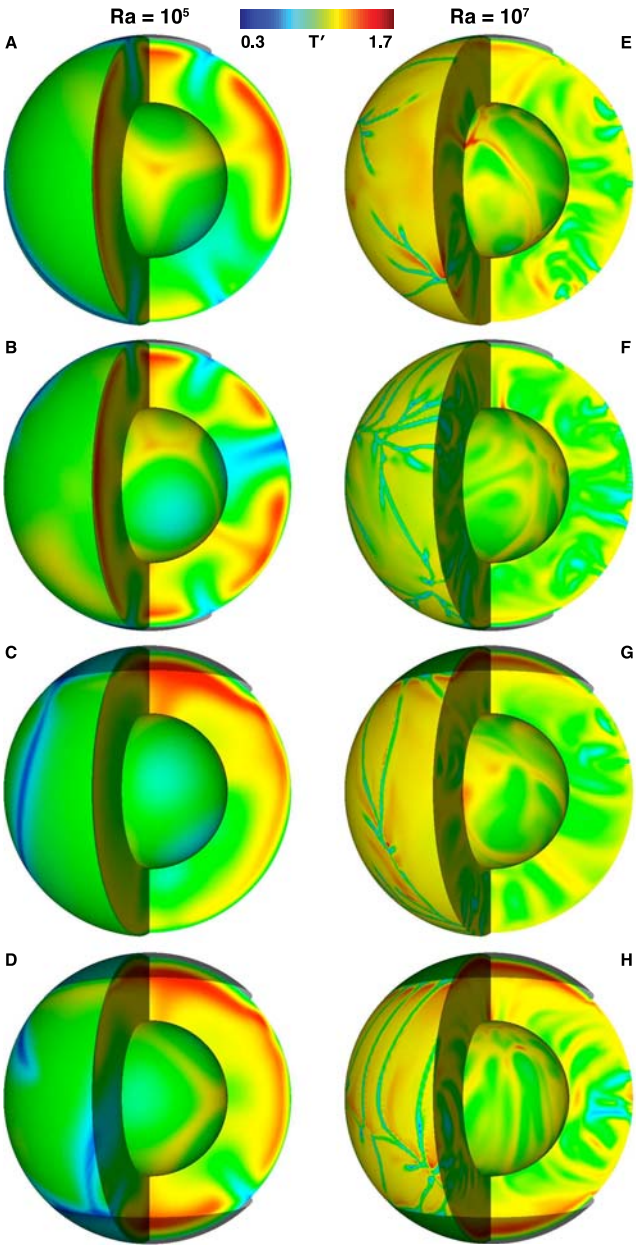

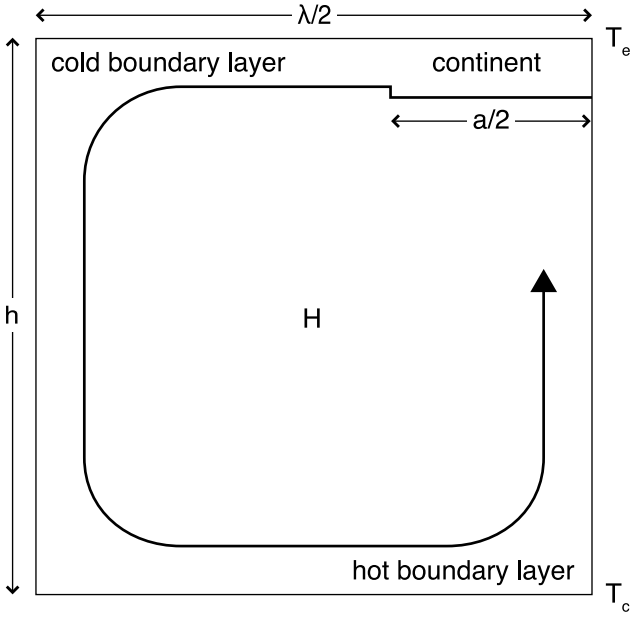

Figure 7. Schematic of a two-dimensional boundary layer convection model. A cell of height h and half-width $\lambda/2$ is partially capped by a continent of half-width $a/2$. The upper and lower boundaries are fixed at temperatures T_e and T_c, respectively, and the fluid is heated uniformly from within at rate H.

5.2. Localized Effect of Continents

[28] Our results show that the temperature beneath isolated, fixed continents depends on individual continent size, independent of total continental cover (Figures 2 and 3). Other numerical and laboratory studies that focused on varying the size of a single continent also record the development of broad upwellings and rising mantle temperatures in the presence of larger continents [e.g., *Gurnis*, 1988; *Guillou and Jaupart*, 1995; *Lowman and Gable*, 1999; *Lenardic et al.*, 2005; *Grigné et al.*, 2007a, 2007b; *Jellinek and Lenardic*, 2009]. The new result here is that the local thermal structure beneath a given continent may be

Figure 6. Snapshots of mantle temperature for eight internally heated models. Continent locations are shown as translucent caps at the poles. Nondimensional temperatures of $T' = 0.3$ to 1.7 are shown in blue to red, respectively. (a) $\mathrm{Ra} = 10^5$ model with a single, small $a'/2 = 0.994$ continent. Multiple convection cells independent of the continent are apparent. (b) As in Figure 6a, but with two small continents. (c) $\mathrm{Ra} = 10^5$ model with a larger $a'/2 = 1.75$ continent. The continent has forced the development of a single, large convection cell, as seen in the spectral plot of Figure 4. (d) The addition of a second $a'/2 = 1.75$ continent arrests the single cell, promoting a planform dominated by two cells. (e) As in Figure 6a, but with $\mathrm{Ra} = 10^7$. Smaller-scale structure is prevalent. (f) As in Figure 6e, but with two continents. (g) $\mathrm{Ra} = 10^7$ model with a single $a'/2 = 1.75$ continent. The broad flow feature associated with the continent has strengthened with respect to the finer-scale structures. (h) As in Figure 6g, but with two continents. A second large cell associated with the second continent is apparent.

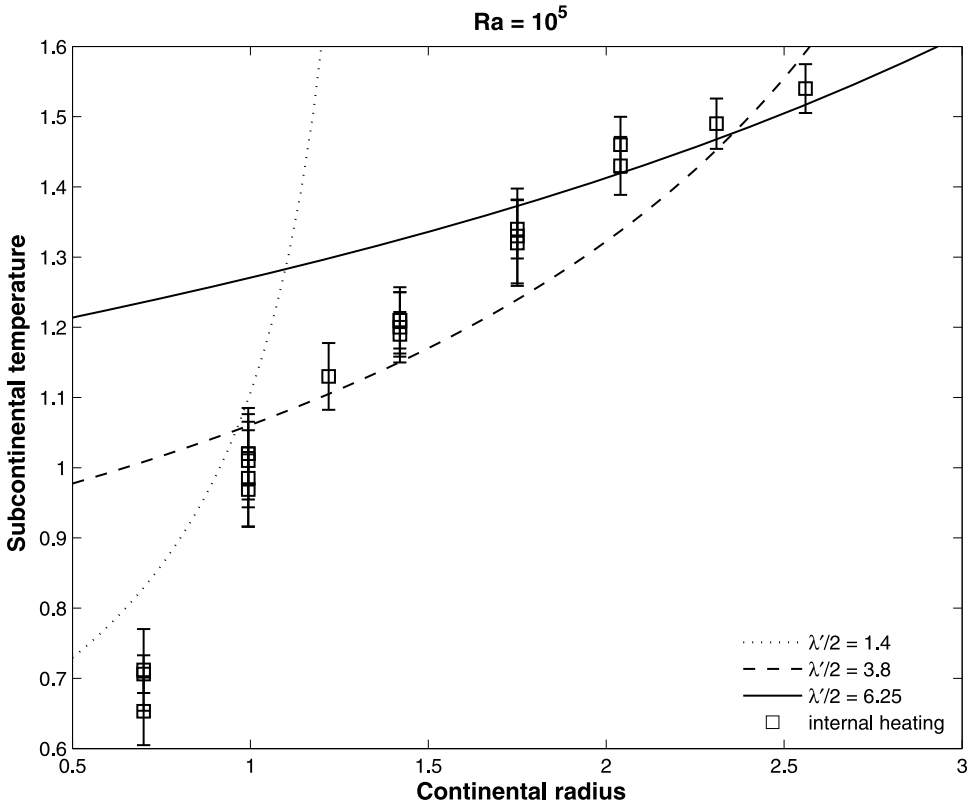

Figure 8. Nondimensional subcontinental temperature as a function of continent size for models with internal heating and Ra = 10^5. Squares mark average temperatures over individual continental footprints just below the thermal boundary layer for all such models run. Dotted, dashed, and solid lines are scaled solutions to equation (8) for small, medium, and large convection cells with nondimensional half-widths of $\lambda'/2$ = 1.4, 3.8, and 6.25, respectively. For small continent size, temperatures fall near the trend associated with the small cell. As continent size increases, temperature jumps to correlate with the trend for larger cells, reaching the largest scale for continents with $a'/2 > 1.42$, in agreement with Figure 4.

unaffected by increasing the total continental cover through the inclusion of additional, dispersed continents. This is not unexpected when considered in the context of the box models of *Guillou and Jaupart* [1995] and *Grigné et al.* [2007b], which both document that normal Rayleigh-Bénard convection can persist away from a continent, with the sphere of influence increasing with lid size and Ra.

[29] The potential for a continent to impact the mantle only locally is further reflected in the spectral content of the temperature fields in our models. At Ra = 10^5, flow in the presence of the smallest continents exhibits a peak in spectral heterogeneity at spherical harmonic degrees 3 and 4 (Figure 4). This indicates the existence of dominant convection cells that are independent of the one or two continents. As continent size increases past $a'/2$ = 1.42, predominant structure moves to degrees 1 or 2, signifying the development of a broad convection cell mated to each continent. In contrast, as Ra increases to 10^7 the number of continents in the model always dictates the dominant time-averaged length scale of flow. The fact that this holds for all continent sizes reinforces the finding of *Grigné et al.* [2007b] that even small continents can promote large-scale flow at high Ra. The increase of viscosity with depth is also a key factor in reinforcing large-scale flow with increasing convective vigor. However, models with a viscously stratified mantle and no continents yield prominent degree 3 to 4 structure [*Bunge et al.*, 1996], not degree 1 to 2 as seen here. So, while it is difficult to isolate which effect (continent or layered viscosity) is dominant, both contribute to the large-scale flow pattern observed at higher Ra. The strength of this large-scale circulation clearly diminishes with respect to the strength of small-scale structure as continent size decreases (Figure 5). We might expect the peak spherical harmonic degree to go back to 3 or 4 as the continent size shrinks to zero. This coupling of convection cells to continents also suggests that the degree 2 structure could represent a sort of forced loop regime [*Grigné et al.*, 2007a] in spherical geometry, where the inhibitor to free convection is not the domain boundary but the diametric flow excited by continents in opposing hemispheres.

[30] As suggested above, small-scale structure certainly persists as an undercurrent to large-scale flow, particularly at large Ra (Figures 4 and 5). This agrees in general with our understanding that vigorous convection supports finer-scale heterogeneities [e.g., *Turcotte and Oxburgh*, 1967] and matches observations that small features commensurate in size with the boundary layer thickness remain even when subjected to overprinting by a broad flow field in the presence of a conducting lid [e.g., *Guillou and Jaupart*, 1995; *Grigné et al.*, 2007b].

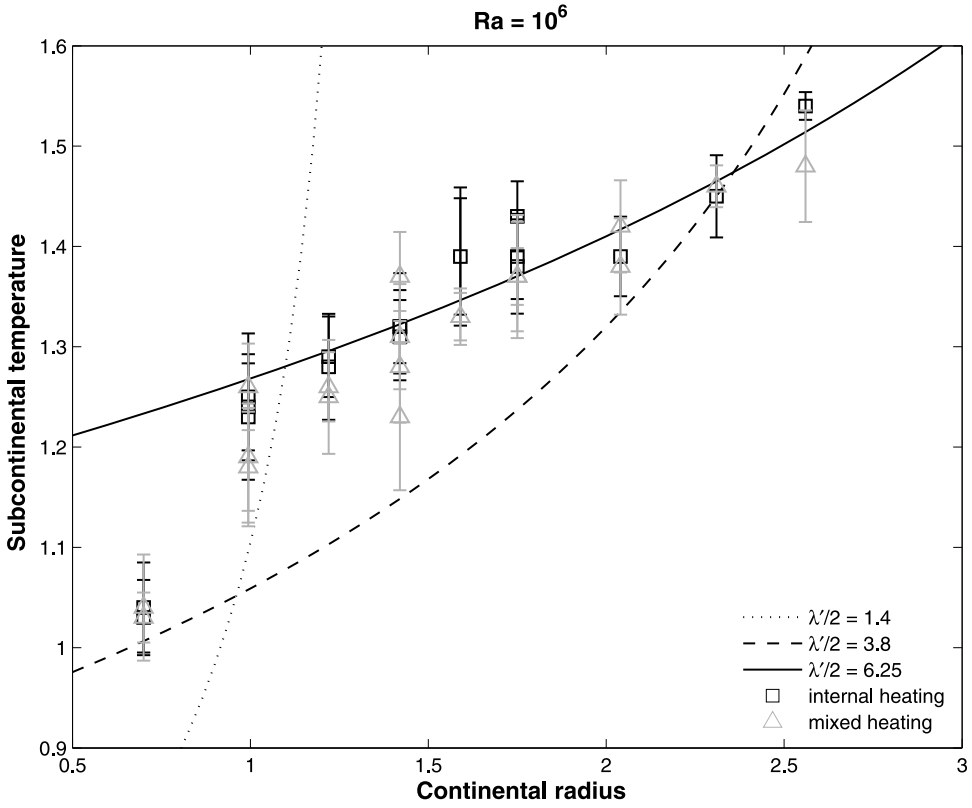

Figure 9. As in Figure 8, except for both purely internally heated (black squares) and 15% core heated (gray triangles) models with Ra = 10^6. Subcontinental temperature follows the trend for long-wavelength convection, except for with the smallest continents.

[31] Despite the simplicity of the analytical model of section 3.3, temperature scalings from equation (8) matched the results of our models well (Figures 8–10). Subcontinental temperature clearly rises with continent size in our models, reflecting mostly the effect of insulation. In addition, this trend overlies a fundamental increase in temperature with convective wavelength. For Ra = 10^5, dominant wavelength increases with continent size, leading to steep increases in temperature due to the compounding effects (Figure 8). The nondimensional circumference of our model domain is roughly $c' = c/h$ = 40,000 km/2890 km = 13.8. The four cell sizes plotted, $\lambda'/2$ = 1.4, 3.8, 6.25, and 7.6 therefore correspond roughly to full convection cells in the sphere with spatial frequency at degrees 5, 2, and 1 (for the two largest values), respectively. As seen in Figure 8, the $a'/2$ = 0.7 continent falls near the degree 5 trend. Referring to the heterogeneity map of Figure 4 we see that the peak time-averaged spectral amplitude is also very nearly 5. As continental radius increases, subcontinental temperature transitions to the degree 2 trend for $a'/2 > 0.99$ and to the degree 1 trend for $a'/2 > 1.42$ (Figure 8). Again this is reflected in the spectral content of the temperature field (Figure 4), strengthening the case that flow scale is an underlying factor in setting the system temperature.

[32] Increasing Ra to 10^6 sparks a transition to larger dominant wavelengths for a given continent size (Figure 9). Degree 2 structure now dominates the $a'/2$ = 0.7 case, with all larger continents falling on the trend for the largest cell. At Ra = 10^7 any dependence on smaller wavelengths is overcome, reflecting the bias toward long wavelengths for high Ra [*Guillou and Jaupart*, 1995; *Grigné et al.*, 2007b]. Correspondingly, temperature increases with continent size following a gentler trend that corresponds to increasing insulation within the bounds of a single flow scale (Figures 5 and 10).

5.3. Time-Dependent Subcontinental Temperature

[33] We see that subcontinental temperature depends on individual continent size and not total continent cover for isolated continents. Clearly as continents approach one another or aggregate, they effectively behave as one larger continent and underlying temperature will increase, as in the case of small continents in some of our three continent models (Figure 3). This is shown also in our mobile continent model of Figure 11. The smaller two continents (gray lines) collide at $t' \sim 80$ and 250, yielding warming trends beneath the aggregated pair. However, continental proximity is transient on the Earth. The mobile model showcases how a particular snapshot such as that for today's Earth may not represent the time-averaged system, while demonstrating that the dependence of subcontinental temperature on size holds when averaged over timescales on the order of 1 Gyr.

[34] Some more subtle features characteristic of a system in which continents interact also appear in the mobile model. For example, the temperature beneath a small continent usually rises when in proximity to a larger continent, despite the fact that the largest continent in the model is

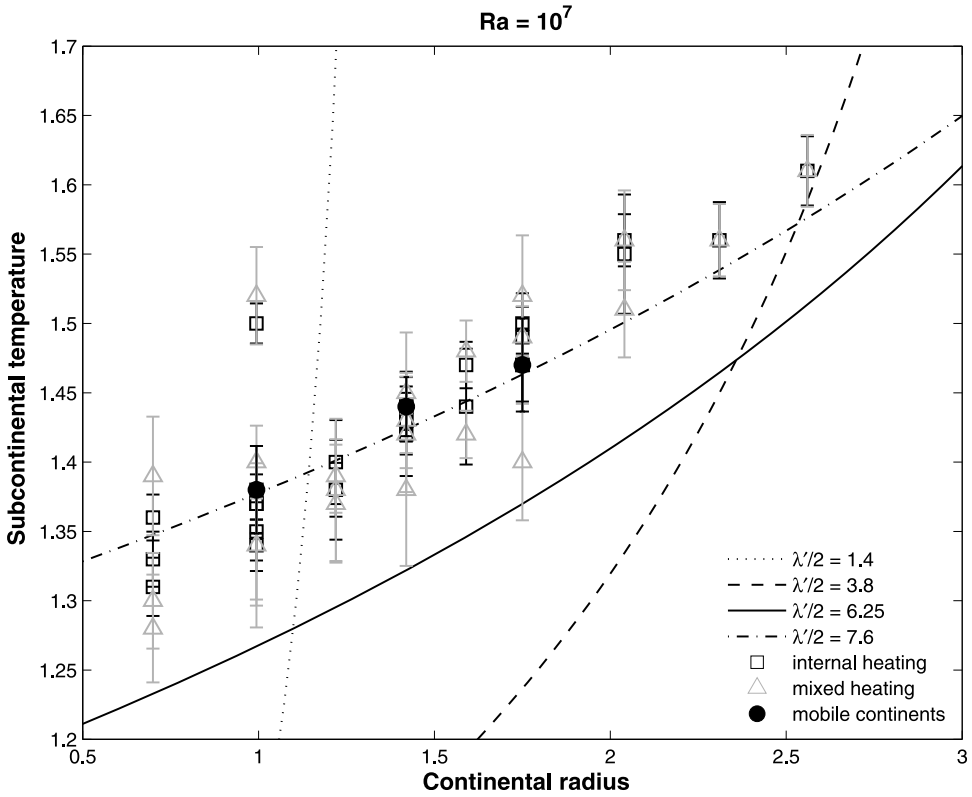

Figure 10. As in Figure 9, except for purely internally heated (black squares) and 15% core heated (gray triangles), fixed continent models and the 15% core heated, mobile continent model (black circles) all with Ra = 10^7. The dash-dot line shows an additional solution to equation (8) for a slightly longer wavelength cell. Subcontinental temperature increases with continent size along the trend for convection at the longest wavelength.

generally colder upon aggregation (Figure 11). The mantle under the large continent, even when relatively cold, is still almost always warmer than that beneath the small continent. And, the fact that the mantle beneath the large continent cools in association with aggregation is not as surprising as it seems. Laterally convergent flow capable of drawing in smaller continents can probably only occur when the large continent has settled on a substantial, cold downwelling.

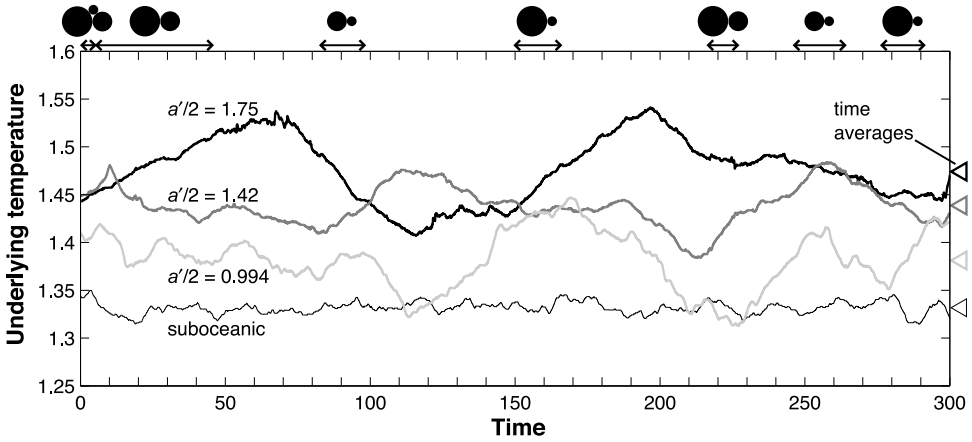

Figure 11. Nondimensional underlying mantle temperature as a function of nondimensional time for a model containing three mobile continents with $a'/2$ = 1.75 (thick black line), 1.42 (dark gray line), and 0.994 (light gray line) in a 15% core heated mantle with Ra = 10^7. The thin black line corresponds to the suboceanic mantle. Triangles on the right mark the average temperature over the full course of the model for each mantle region. Arrows at the top bracket time periods during which continents are aggregated. Black discs indicate by size which continents are in contact. There is significant time variability in subcontinental temperature, but on average, temperature is still a function of continent size.

This is seen at $t' \sim 0$, 150, 220, and 280 in Figure 11, for example.

[35] As shown in Figure 11, the mantle beneath the smallest continent in the mobile model is sometimes colder than the suboceanic mantle ($t' \sim 110$ and 220). While the 70% of the mantle that lies beneath the oceans always harbors a mix of hot, cold, and ambient features (Figure 6), the small continent's diminutive footprint at times overlies only colder mantle. In other words, a small continent integrates temperature over a smaller portion of the mantle than does a larger continent or the oceans, and time dependence ensures that this will sometimes lead to anonymously cold subcontinental temperature.

[36] The mobile model records temperature variations of $T' = 0.10$ to 0.13 for each of the three continents. This corresponds to dimensional changes of roughly 90 to 120°C due to time dependence of the coupled continent-mantle system. Other modeling results [*Coltice et al.*, 2007, 2009] and observations of the African superswell [*Anderson*, 1982] suggest that these variations are expected in response to the redistribution of continents. Such time dependence makes it hard to test the predictions of our results here with respect to the present-day Earth, since at any given time the temperature beneath a particular continent may fall far from its time-averaged trend. A number of observations could, however, help to support or refute the dependence of subcontinental temperature on continent size. The history of dynamic topography [e.g., *Gurnis*, 1993] could carry the signal of this trend. A greater prevalence of volcanoes on larger continents would also support the notion. The preponderance of flood basalt eruptions associated with supercontinents provides a good end-member verification of this observable throughout most of Earth's history [*Yale and Carpenter*, 1998; *Condie*, 2004; *Coltice et al.*, 2009]. Refining this trend over a larger range of continental (or cratonic) sizes would require a significant query of the geologic record. Still, our results provide a good metric for the potential influences of continents and their distribution on the thermal evolution of the mantle.

6. Conclusions

[37] This paper explores some key mechanisms behind mantle warming due to continents. Many numerical and laboratory models that address this problem concentrate on the effect of a single continent, often in Rayleigh-Bénard convection and often in Cartesian geometry. Our models differ from this in that they consider the importance of both the size and distribution of continents as well as their effect on the convective planform of a layered viscosity, spherical mantle heated both from below and within.

[38] We find that subcontinental temperature increases as a function of both continent size and convective wavelength. At a low Rayleigh number of 10^5, temperature increases steeply with size as the effects of larger caps are compounded by progressively longer-wavelength flow. As the Rayleigh number increases to 10^7, the flow scale is broad even in the presence of a small continent, leaving temperature primarily dependent on continent size. For the vigorously convecting Earth we might then expect that a primary dependence on continent size drives variations in time-averaged subcontinental temperature.

[39] **Acknowledgments.** We thank two anonymous reviewers for constructive comments that inspired a clearer manuscript. This work was supported by a Los Alamos National Laboratory Director's Postdoctoral Fellowship and a Visiting Scientist appointment at the National Science Foundation (BRP). Any opinion, findings, and conclusions or recommendations expressed in this material are those of the authors and do not necessarily reflect the views of the National Science Foundation.

References

Anderson, D. L. (1982), Hotspots, polar wander, Mesozoic convection and the geoid, *Nature*, *297*, 391–393.

Anderson, D. L. (1994), Superplumes or supercontinents?, *Geology*, *22*, 39–42.

Artemieva, I. M., and W. D. Mooney (2001), Thermal structure and evolution of Precambrian lithosphere: A global study, *J. Geophys. Res.*, *106*, 16,387–16,414.

Bobrov, A. M., W. Jacoby, and V. P. Trubitsyn (1999), Effects of Rayleigh number, length and thickness of continent on time of mantle flow reversal, *J. Geodyn.*, *27*, 133–145.

Buffett, B. (2002), Estimates of heat flow in the deep mantle based on the power requirements for the geodynamo, *Geophys. Res. Lett.*, *29*(12), 1566, doi:10.1029/2001GL014649.

Bunge, H.-P. (2005), Low plume excess temperature and high core heat flux inferred from non-adiabatic geotherms in internally heated mantle circulation models. *Phys. Earth Planet. Inter.*, *153*, 3–10.

Bunge, H.-P., and J. R. Baumgardner (1995), Mantle convection modeling on parallel virtual machines, *Comput. Phys.*, *9*(2), 207–215.

Bunge, H.-P., and M. A. Richards (1996), The origin of large scale structure in mantle convection: Effects of plate motions and viscosity structure, *Geophys. Res. Lett.*, *23*(21), 2987–2990.

Bunge, H.-P., M. A. Richards, and J. R. Baumgardner (1996), Effect of depth-dependent viscosity on the planform of mantle convection, *Nature*, *379*, 436–438.

Coltice, N., B. R. Phillips, H. Bertrand, Y. Ricard, and P. Rey (2007), Global warming of the mantle at the origin of flood basalts over supercontinents, *Geology*, *35*(5), 391–394.

Coltice, N., H. Bertrand, P. Rey, F. Jourdan, B. R. Phillips, and Y. Ricard (2009), Global warming of the mantle beneath continents back to the Archaean, *Gondwana Res.*, *15*, 254–266, doi:10.1016/j.gr.2008.10.001.

Condie, K. C. (2004), Supercontinents and superplume events: Distinguishing signals in the geologic record, *Phys. Earth Planet. Inter.*, *146*, 319–332.

Cooper, C. M., A. Lenardic, and L. Moresi (2006), Effects of continental insulation and the partitioning of heat producing elements on the Earth's heat loss, *Geophys. Res. Lett.*, *33*, L13313, doi:10.1029/2006GL026291.

Dalton, C. A., G. Ekström, and A. M. Dziewoński (2008), The global attenuation structure of the upper mantle, *J. Geophys. Res.*, *113*, B09303, doi:10.1029/2007JB005429.

Davies, G. F. (1988), Ocean bathymetry and mantle convection: 1. Large-scale flow and hotspots, *J. Geophys. Res.*, *93*, 10,467–10,480.

Davies, G. F. (1999), *Dynamic Earth*, 458 pp., Cambridge Univ. Press, Cambridge, U. K.

Gable, C. W., R. J. O'Connell, and B. J. Travis (1991), Convection in three dimensions with surface plates: Generation of toroidal flow, *J. Geophys. Res.*, *96*, 8391–8405.

Gait, A. D., J. P. Lowman, and C. W. Gable (2008), Time dependence in 3-D mantle convection models featuring evolving plates: Effect of lower mantle viscosity, *J. Geophys. Res.*, *113*, B08409, doi:10.1029/2007JB005538.

Grigné, C., and S. Labrosse (2001), Effects of continents on Earth cooling: Thermal blanketing and depletion in radioactive elements, *Geophys. Res. Lett.*, *28*(14), 2707–2710.

Grigné, C., S. Labrosse, and P. J. Tackley (2007a), Convection under a lid of finite conductivity: Heat flux scaling and applications to continents, *J. Geophys. Res.*, *112*, B08402, doi:10.1029/2005JB004192.

Grigné, C., S. Labrosse, and P. J. Tackley (2007b), Convection under a lid of finite conductivity in wide aspect ratio models: Effect of continents on the wavelength of mantle flow, *J. Geophys. Res.*, *112*, B08403, doi:10.1029/2006JB004297.

Guillou, L., and C. Jaupart (1995), On the effect of continents on mantle convection, *J. Geophys. Res.*, *100*, 24,217–24,238.

Gung, Y., M. Panning, and B. Romanowicz (2003), Global anisotropy and the thickness of continents, *Nature*, *422*, 707–711.

Gurnis, M. (1988), Large-scale mantle convection and the aggregation and dispersal of supercontinents, *Nature*, *332*, 695–699.

Gurnis, M. (1993), Phanerozoic marine inundation of continents driven by dynamic topography above subducting slabs, *Nature*, *364*, 589–593.

Hager, B. H., and M. A. Richards (1989), Long-wavelength variations in Earth's geoid: Physical models and dynamical implications, *Philos. Trans. R. Soc. London, Ser. A*, *328*, 309–327.

Jellinek, A. M., and A. Lenardic (2009), Effects of spatially varying roof cooling on generation of long wavelength heterogeneity in the mantle in a fluid with a strongly temperature-dependent viscosity, *J. Fluid Mech.*, *629*, 109–138.

Kellogg, L. H., B. H. Hager, and R. D. van der Hilst (1999), Compositional stratification in the deep mantle, *Science*, *283*, 1881–1884.

Lenardic, A., and W. M. Kaula (1995), Mantle dynamics and the heat flow into the Earth's continents, *Nature*, *378*, 709–711.

Lenardic, A., L.-N. Moresi, and H. Mühlhaus (2003), Longevity and stability of cratonic lithosphere: Insights from numerical simulations of coupled mantle convection and continental tectonics, *J. Geophys. Res.*, *108*(B6), 2303, doi:10.1029/2002JB001859.

Lenardic, A., L.-N. Moresi, A. M. Jellinek, and M. Manga (2005), Continental insulation, mantle cooling, and the surface area of oceans and continents, *Earth Planet. Sci. Lett.*, *234*, 317–333.

Le Pichon, X., and P. Huchon (1984), Geoid, Pangea and convection, *Earth Planet. Sci. Lett.*, *67*, 123–135.

Lithgow-Bertelloni, C., and M. A. Richards (1998), The dynamics of Cenozoic and Mesozoic plate motions, *Rev. Geophys.*, *36*, 27–28.

Lowman, J. P., and C. W. Gable (1999), Thermal evolution of the mantle following continental aggregation in 3D convection models, *Geophys. Res. Lett.*, *26*(17), 2649–2652.

Lowman, J. P., and G. T. Jarvis (1993), Mantle convection flow reversals due to continental collisions, *Geophys. Res. Lett.*, *20*(19), 2087–2090.

Monnereau, M., and S. Quéré (2001), Spherical shell models of mantle convection with tectonic plates, *Earth Planet. Sci. Lett.*, *184*, 575–587.

Nolet, G., S. I. Karato, and R. Montelli (2006), Plume fluxes from seismic tomography, *Earth Planet. Sci. Lett.*, *248*, 685–699.

Phillips, B. R., and H.-P. Bunge (2005), Heterogeneity and time dependence in 3D spherical mantle convection models with continental drift, *Earth Planet. Sci. Lett.*, *233*, 121–135.

Phillips, B. R., and H.-P. Bunge (2007), Supercontinent cycles disrupted by strong mantle plumes, *Geology*, *35*(9), 847–850.

Phillips, B. R., H.-P. Bunge, and K. Schaber (2009), True polar wander in mantle convection models with multiple, mobile continents, *Gondwana Res.*, *15*, doi:10.1016/j.gr.2008.11.007.

Ricard, Y., M. Richards, C. Lithgow-Bertelloni, and Y. Le Stunff (1993), A geodynamic model of mantle density heterogeneity, *J. Geophys. Res.*, *98*, 21,895–21,909.

Sclater, J. G., C. Jaupart, and D. Galson (1980), The heat flow through oceanic and continental crust and the heat loss of the Earth, *Rev. Geophys. Space Phys.*, *18*(1), 269–311.

Tackley, P. J. (2000), Self-consistent generation of tectonic plates in time-dependent, three-dimensional mantle convection simulations: 2. Strain weakening and asthenosphere, *Geochem. Geophys. Geosyst.*, *1*(8), 1026, doi:10.1029/2000GC000043.

Trubitsyn, V. P., and V. V. Rykov (1995), A 3-D numerical model of the Wilson cycle, *J. Geodyn.*, *20*(1), 63–75.

Trubitsyn, V. P., and V. V. Rykov (2001), A numerical evolutionary model of interacting continents floating on a spherical Earth, *Russ. J. Earth Sci.*, *3*(2), 83–95.

Trubitsyn, V., M. K. Kaban, and M. Rothacher (2008), Mechanical and thermal effects of floating continents on the global mantle convection, *Phys. Earth Planet. Inter.*, *171*, 313–322.

Turcotte, D. L., and E. R. Oxburgh (1967), Finite amplitude convective cells and continental drift, *J. Fluid Mech.*, *28*, 29–42.

Turcotte, D. L., and G. Schubert (2002), *Geodynamics*, 2nd ed., 456 pp., Cambridge Univ. Press, Cambridge, U. K.

van Heck, H. J., and P. J. Tackley (2008), Planforms of self-consistently generated plates in 3D spherical geometry, *Geophys. Res. Lett.*, *35*, L19312, doi:10.1029/2008GL035190.

van Keken, P. (2001), Cylindrical scaling for dynamical cooling models of the Earth, *Phys. Earth Planet. Inter.*, *124*, 119–130.

Wasserburg, G. J., G. J. F. MacDonald, F. Hoyle, W. A. Fowler (1964), Relative contributions of uranium, thorium, and potassium to heat production in the Earth, *Science*, *143*, 465–467.

Woodhouse, J. H., and A. M. Dziewoński (1984), Mapping the upper mantle: Three-dimensional modeling of Earth structure by inversion of seismic waveforms, *J. Geophys. Res.*, *89*, 5953–5986.

Yale, L. B., and S. J. Carpenter (1998), Large igneous provinces and giant dike swarms: Proxies for supercontinent cyclicity and mantle convection, *Earth Planet. Sci. Lett.*, *163*, 109–122.

Yoshida, M., Y. Iwase, and S. Honda (1999), Generation of plumes under a localized high viscosity lid in 3-D spherical shell convection, *Geophys. Res. Lett.*, *26*(7), 947–950.

Zhong, S., and M. Gurnis (1993), Dynamic feedback between a continent-like raft and thermal convection, *J. Geophys. Res.*, *98*, 12,219–12,232.

Zhong, S., N. Zhang, Z.-X. Li, and J. H. Roberts (2007), Supercontinent cycles, true polar wander, and very long-wavelength mantle convection, *Earth Planet. Sci. Lett.*, *261*, 551–564.

N. Coltice, Laboratoire de Sciences de la Terre, UMR 5570, Université Lyon 1, CNRS, Bat Géode, 2 rue Raphael Dubois, F-69622 Villeurbanne CEDEX, France. (coltice@univ-lyon1.fr)

B. R. Phillips, Earth and Environmental Sciences Division, Los Alamos National Laboratory, Los Alamos, NM 87545, USA. (benp@lanl.gov)